

New precision measurement of the J/ψ - and ψ' -meson masses*

V.M. Aulchenko, S.A. Balashov, E.M. Baldin,[†] M.Yu. Barnyakov, S.E. Baru, I.V. Bedny, O.L. Beloborodova, A.E. Blinov, V.E. Blinov, A.V. Bogomyagkov, A.E. Bondar, D.V. Bondarev, A.R. Buzykaev, S.I. Eidelman, V.R. Groshev, S.E. Karnaev, V.A. Kiselev, S.A. Kononov, K.A. Kotov, E.A. Kravchenko, E.V. Kremyanskaya, E.B. Levichev, V.M. Malyshev, A.L. Maslennikov, O.I. Meshkov, S.E. Mishnev, N.Yu. Muchnoi, A.I. Naumenkov, S.A. Nikitin, I.B. Nikolaev, A.P. Onuchin, S.B. Oreshkin, Yu.A. Pakhotin, S.V. Peleganchuk, S.S. Petrosyan, V.V. Petrov, A.O. Poluektov, A.A. Polunin, G.E. Pospelov, I.Ya. Protopopov, G.A. Savinov, A.G. Shamov, D.N. Shatilov, A.I. Shusharo, B.A. Shwartz, V.A. Sidorov, E.A. Simonov, Yu.I. Skovpen, A.N. Skrinsky, A.M. Soukharev, A.A. Talyshev, V.A. Tayursky, V.I. Telnov, Yu.A. Tikhonov, K.Yu. Todyshev, G.M. Tumaikin, Yu.V. Usov, A.I. Vorobiov, A.N. Yushkov, A.V. Zatsepin, and V.N. Zhilich
KEDR Collaboration. Budker Institute of Nuclear Physics, 630090 Novosibirsk, Russia

A new high precision measurement of the J/ψ - and ψ' -meson masses has been performed at the VEPP-4M collider using the KEDR detector. The resonant depolarization method has been employed for the absolute calibration of the beam energy. The following mass values have been obtained:

$$\begin{aligned} M_{J/\psi} &= 3096.917 \pm 0.010 \pm 0.007 \text{ MeV}, \\ M_{\psi'} &= 3686.111 \pm 0.025 \pm 0.009 \text{ MeV}. \end{aligned}$$

The relative measurement accuracy has reached $4 \cdot 10^{-6}$ for J/ψ and $7 \cdot 10^{-6}$ for ψ' , approximately 3 times better than in the previous precise experiments.

I. INTRODUCTION

This work continues a series of experiments on the precise determination of the onium resonance masses at the electron-positron collider VEPP-4: J/ψ , ψ' (OLYA detector) [1] and Υ , Υ' , Υ'' (MD-1 detector) [2, 3, 4, 5]. A few years ago the values of the masses obtained have been rescaled [6, 7] to take into account the progress in the electron mass measurements [8, 9].

VEPP-4 experiments employed the resonant depolarization method [10, 11] for the absolute beam energy calibration and achieved the relative mass accuracy of $1 \cdot 10^{-5}$ for the Υ -family and of $3 \cdot 10^{-5}$ for the ψ -family. The resonant depolarization experiments on bottomonium masses were also performed with the CUSB detector at CESR [12] (Υ) and with the ARGUS detector at DORIS [13] (Υ'). The accuracy of the J/ψ -mass measurement was improved in the Fermilab $p\bar{p}$ -experiment E760 [14] to $1.2 \cdot 10^{-5}$ using the ψ' mass value from Ref. [1].

The goals of this work were to further improve the accuracy of the J/ψ - and ψ' -masses and develop the resonant depolarization technique at the upgraded VEPP-4M collider for future experiments.

The first precise measurement of the J/ψ and ψ' meson masses [1] set the mass scale in the range around 3 GeV which provided a basis for the accurate determination of the charmonium state location. At present the charm meson family is a good test bench for QCD and

quark potential models predictions in which masses of the open and hidden charm can be calculated with good accuracy. Another fundamental application of the mentioned measurements is the τ -lepton mass determination [15].

Substantial improvement in the beam energy accuracy obtained by the presented experiment sets a new standard of the mass scale in the charmonium range.

II. BEAM ENERGY DETERMINATION TECHNIQUE

A. Resonant depolarization method

Electrons and positrons in storage rings can become polarized due to emission of synchrotron radiation according to the Sokolov-Ternov effect [16]. Spins of polarized electrons precess around the vertical guiding magnetic field with the precession frequency Ω , which in the plane orbit approximation is directly related to the particle energy E and the beam revolution frequency ω :

$$\Omega/\omega = 1 + \gamma \cdot \mu'/\mu_0 = 1 + \nu, \quad (1)$$

where $\gamma = E/m_e$, m_e is the electron mass, μ' and μ_0 are the anomalous and normal parts of the electron magnetic moment. The ν is a spin tune, which represents the spin precession frequency in the coordinate basis related to the particle velocity vector.

The precession frequency can be determined using the *resonant depolarization*. To this end one needs a polarized beam in the storage ring which is affected by the external electromagnetic field with the frequency Ω_D given by the relation

$$\Omega \pm \Omega_D = \omega \cdot n \quad (2)$$

*Partially supported by the Russian Foundation for Basic Research, Grants 01-02-17477, 02-02-16321, 02-02-17321 and the Presidential Grants 1335.2003.2, 1346.2003.2 for support of Leading Scientific Schools.

[†]e-mail: E.M.Baldin@inp.nsk.su (corresponding author)

with any integer n (for VEPP-4M in the J/ψ region $n = 3$).

The precession frequency is measured at the moment of the polarization destruction detected by the *polarimeter*, while the *depolarizer* frequency is being scanned. The process of forced depolarization is slow enough compared to the period of the synchrotron oscillations of the particle energy. This allows to determine the average spin tune $\langle\nu\rangle$ and corresponding average energy of the particles $\langle E\rangle$ with higher accuracy than the beam energy spread σ_E .

Due to modulation of the precession frequency by particle orbital motion, the resonant depolarization could happen at the sideband resonances, which are distant from the main one by multiples of the synchrotron and betatron frequencies. Besides, it could happen at the weak sideband resonances caused by extraneous low frequency modulation of the guide field, caused for example by pulsations in the power supply system (50 Hz, the energy shift of about 25 keV). Therefore, it is necessary to identify the main resonance by special means.

It should be noted that the average energy of the beam particles $\langle E\rangle$ differs from the energy of the equilibrium particle E_s because of the radial betatron oscillations. The effect is proportional to the betatron amplitude squared and is mainly due to the nonlinearity of the guide field. It also determines the spin resonance natural bandwidth [17]. In this experiment the observed full bandwidth was about 5 keV in beam energy units.

Formula (1) gives the value of γ averaged over the beam revolution time. Thus, for a symmetric machine, it corresponds to the energy in the interaction point.

The method described has been developed in Novosibirsk and first applied to the ϕ -meson mass measurement at the VEPP-2M storage ring [10]. The comprehensive review of the resonant depolarization technique and its applications for particle mass measurements can be found in [18].

B. VEPP-4M polarimeter

The polarimeter unit is installed in the technical straight section of VEPP-4M and consists of the polarimeter employing the spin dependence of the intra-beam scattering (Touschek) effect [19] and TEM wave-based depolarizer [20].

The polarimeter detects Touschek electron pairs with the help of two movable scintillation counters placed inside the beam pipe pockets. We use the “two bunches” compensation technique, in which relative rates of scattered particles from unpolarized and polarized beams are compared.

The rate of Touschek electrons is $3 \div 12$ kHz at the beam current of $2 \div 4$ mA. The depolarizer frequency is scanned with a step of 2 Hz by the computer controlled synthesizer with the intrinsic bandwidth of ~ 1 Hz. However, the frequency line is artificially broadened up to the

4 Hz band. This provides controllable conditions [21] for the depolarization at the main spin resonance at the minimal level of the depolarizer power, which corresponds to $\sim 2 \cdot 10^{-6}$ rad spin rotation per a single pass of the particle, and with the frequency-tuning rate of 0.2 Hz/sec.

The characteristic jump in the relative rate of scattered electrons at the moment of resonant depolarization is $3.0 \div 3.5\%$ with the statistical error of $0.3 \div 0.4\%$ for the beam polarization degree higher than 50%. Typical behavior of the rate ratio is shown in Fig. 1. The linear growth before the depolarization reflects the difference in the bunch life times due to polarization dependence of the intra-beam scattering cross section.

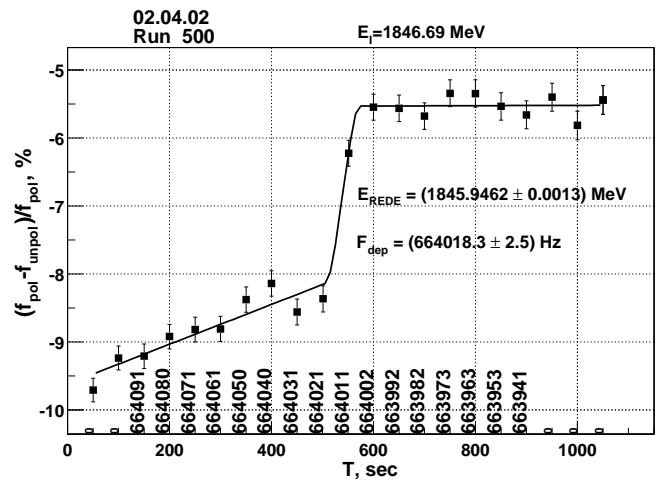


FIG. 1: The variation of the coincidence rate ratio for polarized and unpolarized beams during the energy calibration (E_I is the energy calculated from the magnet currents, E_{REDE} is the energy determined by resonant depolarization, F_{dep} is the corresponding depolarizer frequency; the vertical numbers show the instant depolarizer frequency).

The characteristic uncertainty of the beam energy calibration due to the depolarization procedure is 1.5 keV (for more detail see Ref. [20]).

C. Accuracy of single energy calibration

The achievable accuracy of the J/ψ and ψ' mass measurement was analyzed in [22]. Since that time, understanding of some systematic effects improved. In particular, the energy shift due to the *vertical closed orbit disturbances* turned out to be much less than was expected in [21] and [22].

The relation (1) is broken in the radial magnetic field and the vertical electric field (used for the electrostatic beam separation) because of the orbit non-planarity. The influence of these fields in the second order of perturbation theory can be expressed in terms of Fourier harmonics of the vertical closed orbit disturbances. The accurate analysis of the effect and the numerical simu-

lation gave the energy shift of -0.4 ± 0.3 keV for J/ψ and -0.3 ± 0.2 keV for ψ' .

The uncertainty estimates for the *mean value of the beam energy in the interaction point* for a single calibration are collected in Table I.

The energy value obtained in a single calibration is biased due to a *non-zero spin resonance width*. The required correction (≈ 2.5 keV) can be determined with accuracy better than 1 keV using a few calibrations with opposite directions of the depolarizer frequency scan.

The *coherent energy loss asymmetry* arises from the difference of the resistive impedance of the beam pipe in two half-rings. As a result, the energy of electrons and positrons in the interaction point (I.P.) differs from the energy value obtained by the resonant depolarization.

The uncertainties not exceeding 0.1 keV are not shown in the table including those due to the *non-zero momentum compaction factor* and the *longitudinal magnetic fields* [22].

The *uncertainty of a single energy measurement* does not directly contribute to the *systematic error of the meson mass*. Thus, the effect of the *energy loss asymmetry* in the half-rings has an opposite sign for e^+ and e^- and cancels in the linear approximation. The contribution of the *precession and revolution frequency measurements* has mainly statistical nature and becomes negligible when a large number of calibrations is used. At the same conditions the uncertainty due to the *non-zero spin resonance width* vanishes provided that frequency scan directions alternate.

On the other hand, new sources of the systematic error come into play when a long-term experiment with colliding beams is considered. This is discussed below in Sec. IV B, Sec. V and, finally, Sec. VIII, when the essential features of the experiment are described.

III. EXPERIMENT DESCRIPTION

The first part of the experiment consisted of three scans of the J/ψ -region (the integrated luminosity $\int Ldt \approx 40$ nb $^{-1}$, the beam energy spread $\sigma_E \approx 0.6$ MeV) and three scans of the ψ' -region ($\int Ldt \approx 76$ nb $^{-1}$, $\sigma_E \approx 0.9$ MeV). Then the betatron and synchrotron damping decrements of VEPP-4M were rearranged to reduce the energy spread to 0.45 MeV and the fourth scan of J/ψ was performed ($\int Ldt \approx 10$ nb $^{-1}$). The goal was to verify possible systematic errors related to the collider operating mode and the beam energy spread.

The beam polarization time in the VEPP-4M ring is about 100 hours at the ψ -energy region. For the energy calibration runs, the beam spent the time sufficient for the polarization in the booster ring VEPP-3 (2.5 hours at J/ψ and about 1 hour at ψ') and was injected to VEPP-4M without essential loss of the polarization degree.

During the scan the data were collected at 7 points of the resonance excitation curve (Fig. 2). At points 1

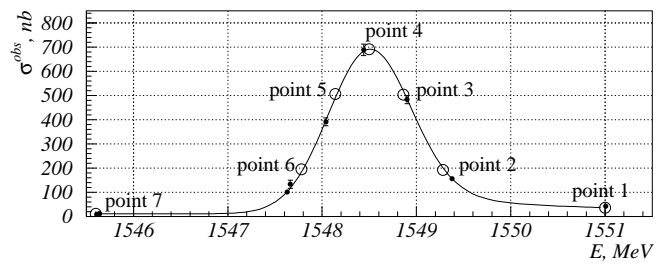


FIG. 2: The data acquisition scenario for J/ψ (circles) and the actual points of the second scan (points with error bars). The solid line shows the second scan fit.

and 7 the required integrated luminosity was reduced by the factor of 2. Such a 5 + 2 scheme does not minimize statistical and systematic errors for a given experiment duration but allows one to apply the χ^2 criterion to the results of a single scan.

Before data acquisition at point 1, the beam energy calibration was made to fix the current energy scale. At points 2–6 the calibrations before and after data taking were performed with the opposite direction of the depolarizer frequency scan. The point 7 requires no energy calibration. From 2 to 5 ring fillings were necessary at each point to collect the wanted integrated luminosity. The injection from VEPP-3 occurred at the required set-up energy without any intentional change of the VEPP-4M magnet currents.

On completion of the scan, the VEPP-4M magnetization cycle was performed and the whole procedure was repeated.

The set-up parameters of the collider and the results of the current, magnetic field, temperature and orbit measurements have been stored in the database.

IV. ASSIGNMENT OF ENERGY TO DATA ACQUISITION RUNS

Unlike the experiments [2, 3, 4], the energy calibration during the data acquisition was not possible, therefore it was necessary to assign the energy to each data acquisition run using the results of the energy calibration runs.

A. Stability runs and energy prediction function

To make the reliable energy assignment, two *stability runs* consisting of the continuous series of energy calibrations without any intentional magnet current changes were performed, one after the third scan of ψ' (March 2002) at the beam energy $E \approx 1846$ MeV [23] and the other one after the fourth scan of J/ψ (May 2002) at $E \approx 1550.6$ MeV. Their results are presented in Figs. 3,4.

One can see a rather slow energy variation and the day-to-night oscillation with the amplitude growing from

TABLE I: Single energy calibration uncertainties in the vicinity of J/ψ and ψ' (keV).

Source	Nature	J/ψ	ψ'
Vertical orbit disturbances	Systematic	0.3*	0.2*
Spin resonance width	Systematic, depends on the frequency scan direction	1.0*	1.0*
Coherent energy loss asymmetry	Systematic, charge depending	0.6	1.
Precession frequency measurement accuracy	Statistical	1.2	1.5
Revolution frequency measurement accuracy of 10^{-8}	Statistical	0.2	0.2
<i>Sum in quadrature</i>		1.7	2.1

* — correction uncertainty

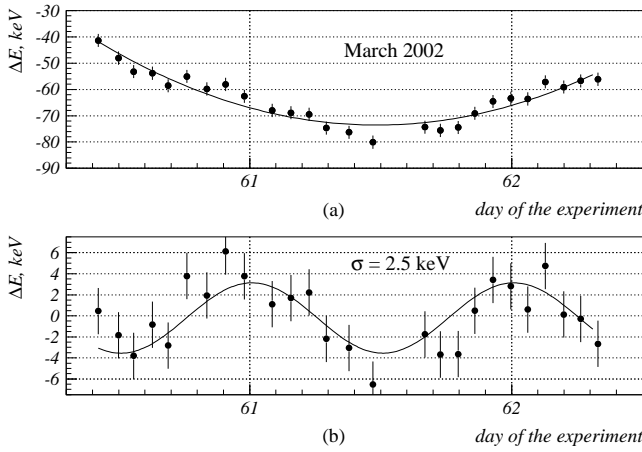


FIG. 3: The results of the first stability run: (a) — parabolic fit of the energy deviation, (b) — the same with the fit subtracted (the error bars show the mean deviation from this fit).

4 keV in March to 45 keV in May. The energy oscillations with the amplitude of (45 ± 5) keV observed since the 110th day of the experiment are correlated with time dependence of the average orbit position with the amplitude of $\Delta R = (51 \pm 10)$ μm . The estimate of the corresponding energy deviation is (77 ± 15) keV under the assumption that the collider expands and shrinks uniformly.

The large and relatively fast energy variations do not allow us to use the mean energy of the two calibrations surrounding a data acquisition run as the beam energy for this run, as was supposed initially. Instead, *energy prediction functions* have been suggested, which employ the results of the field measurements in some magnets by nuclear magnetic resonance (NMR) and the temperature measurements and include the explicit time dependence as a substitute of variables, which were not monitored (the effect of the tunnel wall temperature on the ring perimeter etc.). The orbit measurements at VEPP-4M are not accurate and comprehensive enough to be used for the energy prediction (there are ten independent bending magnet power supplies, sixty radial correctors and only fifty four beam position monitors).

Several prediction functions have been tried of the

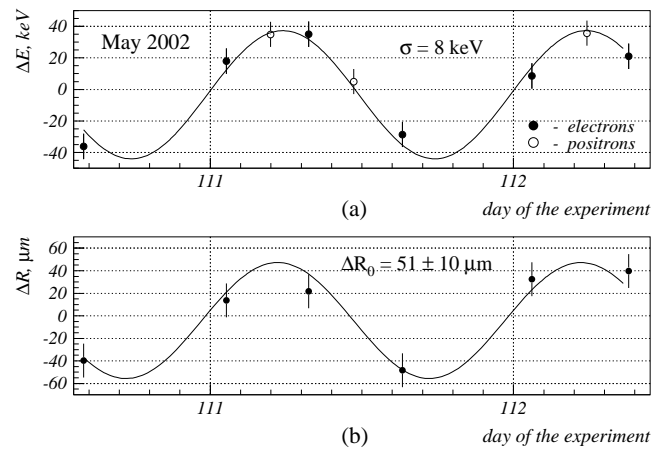


FIG. 4: The results of the second stability run: (a) — energy deviation, (b) — the average orbit position given by BPMs where available (the error bars show the mean deviation from the fit).

form:

$$\begin{aligned}
 E_p = & \mathcal{P} \cdot H_{NMR} \cdot (1 + \varkappa \cdot (T_{ring} - T_{NMR})) \times \\
 & f(T_{ring}, T_{air}, T_{water}) + \\
 \delta E_{on} \cdot \exp\left(-\frac{t_{on}}{\tau_{on}}\right) + & \delta E_{cycle} \cdot \exp\left(-\frac{t_{cycle}}{\tau_{cycle}}\right) + \quad (3) \\
 A(t) \cdot \cos\left(\frac{2\pi t}{\tau} - \varphi(t)\right) + & E_0(\Delta i, t),
 \end{aligned}$$

where H_{NMR} is the field in the off-ring calibration magnet with the temperature of T_{NMR} ; T_{ring} , T_{air} and T_{water} are the average values of the ring and cooling agent temperatures, t is current time, t_{on} and t_{cycle} denote time elapsed since the last switching on the collider and the last magnetization cycle, respectively. The \mathcal{P} , \varkappa , δE_{on} , δE_{cycle} , τ_{on} , τ_{cycle} and τ are free parameters determined by the fit of all energy calibrations performed in a certain operation mode (J/ψ scans I–III, ψ' , J/ψ scan IV).

The first term is the basic parameterization of the magnetic field integral behavior. The exponential terms introduce the magnetic field relaxation; ignoring this effect results in a bias in the parameters \mathcal{P} , \varkappa etc. The oscillating term describes the variations of the ring perimeter under the assumption that the Fourier harmonics around

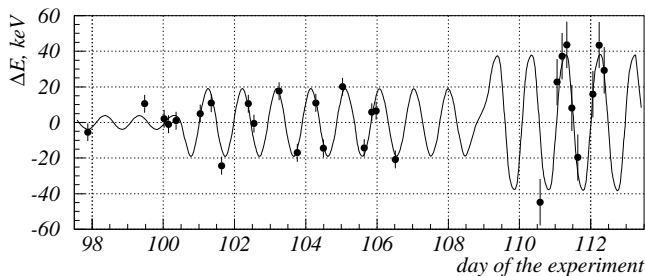


FIG. 5: The predicted energy with all aperiodic dependences removed (the error bars show the mean deviation from the prediction).

$\Omega = 2\pi/\tau$ dominate. The A and φ are not constant due to season variations in properties of the ground surrounding the machine tunnel. The term $E_0(\Delta i, t)$ takes into account the energy variation due to a few relatively large adjustments of the current Δi in some machine lattice elements.

The prediction functions differ by the choice of $f(T)$, $A(t)$ and $\varphi(t)$. These (simplest) functions, as well as $E_0(\Delta i, t)$, have additional free parameters.

The results of the best energy prediction for May 2002 (the fourth scan of J/ψ and the second stability run) are illustrated by Figs. 5 and 6. It should be noted that the time dependence presented in Fig. 6 is partially compensated by the temperature and field strength dependences. Fourteen free parameters were used to fit 28 points shown in these figures. The value of the chi-squared per degree of freedom was employed to estimate the (mean) error of the energy prediction by requiring $\chi^2/N_{DoF} = 1$. According to the fit, the energy oscillation period $\tau = 1.02 \pm 0.02$ days, so we have fixed it at the value of 1.

The appearance of strong oscillations (Fig.5, the 100th day of the experiment) and their further growth (between 107th and 110th days) can be probably explained by the change of the thermomechanical properties of the ground surrounding the half-ring tunnels. These properties can change abruptly at the moment when the melting front reaches the tunnel (in Novosibirsk it occurs in May). According to the χ^2 criterion, the sudden growth of the oscillation amplitude on the 100th day is much more probable than the gradual one.

The direction of the depolarizer frequency scan was taken into account in the prediction function fit. This allows us to determine the spin resonance half-width of 2.4 ± 0.7 keV in beam energy units and makes the prediction function value unbiased. The accuracy of the energy prediction varies from 6 to 8 keV during the whole experiment (218 calibrations).

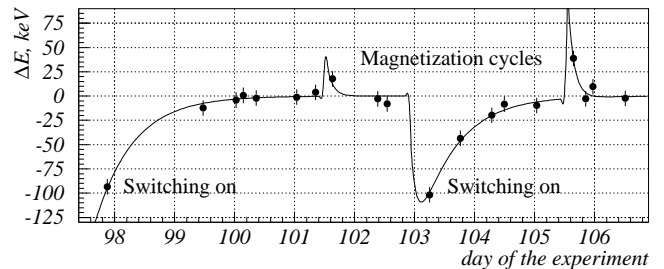


FIG. 6: Aperiodic energy dependence on time due to switching on the ring and the magnetization cycles (the error bars show the mean deviation from the predicted energy).

B. Energy assignment accuracy

The uncertainty of the energy prediction of $(6 \div 8)$ keV includes the *statistical error of the single energy calibration* and all the *uncertainties due to the run-to-run difference*. Among the sources of the latter, the *radial closed orbit variations* and the *RF frequency drift* dominate [22]. The model of statistically independent orbit perturbations used in [22] overestimates the effect of the radial closed orbit variations.

The significant difference between the energy calibration runs and the data acquisition runs was the beam separation at the additional interaction point. This separation could cause some small sign-of-charge dependent shift of the e^+ - and e^- -beam energy. *During the calibrations, the separation was turned off*, so in the linear approximation the energy of the single beam is equal to the mean energy of two beams with the separation on. *During the data acquisition, the separation was turned on* to provide normal conditions for beam-beam effects. This increases the length of the beam orbit in the straight section and decreases it in the half-rings causing the equal energy shift for the e^+ - and e^- -beams. The estimated *energy shifts are* (-1.7 ± 0.2) keV at J/ψ and (-2.0 ± 0.2) keV at ψ' .

Due to the collision effects, the amplitude of the radial betatron oscillations in the data acquisition runs is bigger than that during the energy calibration, therefore, the average particle energies are not the same (see Sec. II A). The corresponding systematic errors of the energy assignment do not exceed 1.5 keV for J/ψ and 1.8 keV for ψ' .

With the two exceptions mentioned above, the energy calibration runs and the data acquisition runs do not differ essentially and we assume the same *statistical accuracy* of the energy prediction for them.

Estimates of the beam energy uncertainty for the data acquisition runs are presented in Table II. The statistical component of the beam energy uncertainty contributes to the meson mass error with the factor $\propto 1/\sqrt{N}$, where N is the number of calibrations. The accurate calculation of this contribution as well as that due to the choice of the energy prediction function can be performed using

TABLE II: The energy uncertainty for the data acquisition runs in the vicinity of J/ψ and ψ' (keV).

Source	Nature	J/ψ	ψ'
Energy prediction	Statistical	7.6	6.5
Radial betatron oscillations	Systematic	< 0.7	< 0.9
Single energy calibration (Sec. II C)	Systematic	0.3	0.2
	Charge depending	0.6	1.0
Beam separation in the additional I.P.	Systematic	0.2*	0.2*
<i>Sum in quadrature</i>		≈ 7.7	≈ 6.6

* — correction uncertainty

the actual resonance curve fit (see Sec. VIII).

V. DETERMINATION OF MEAN COLLISION ENERGY

The production rate of the resonance of mass M at the given collider energy E is determined by the probability of e^+e^- -collisions with the invariant mass $W \simeq M$. Taking the angular spreads θ_x, θ_y and the energy spread σ_E into account, one has after averaging over the particle momenta

$$\langle W \rangle_p \approx \langle E_+ + E_- \rangle - \frac{1}{2}(\theta_x^2 + \theta_y^2)E - \frac{\sigma_E^2}{2E} - \frac{(\langle E_+ \rangle - \langle E_- \rangle)^2}{4E}. \quad (4)$$

The value of E is determined by the resonant depolarization; the last term is due to the difference of the coherent energy loss in two half-rings (Sec. II C). For the VEPP-4M conditions at the ψ -energy region the correction is about 0.2 keV, thus we assume $W = E_+ + E_-$ for each collision.

For beams with the Gaussian energy spread in the presence of the electrostatically induced vertical dispersion ψ_y^* and the beam impact parameter Δ_y , the differential luminosity can be written as

$$\frac{dL(E, W)}{dW} = \frac{f_R N_+ N_-}{4\pi\sigma_x^*(W/2)\sigma_y^*(W/2)} \cdot \frac{1}{\sqrt{2\pi}\sigma_W} \times \exp\left\{-\frac{1}{2}\left(\frac{W-2E}{\sigma_W} - \frac{\sigma_W\psi_y^*\Delta_y}{2E\sigma_y^2}\right)^2 - \frac{\Delta_y^2}{4\sigma_y^2}\right\}, \quad (5)$$

where f_R is a revolution frequency, N_+ and N_- are the bunch populations. The transverse beam sizes in the interaction point σ_x^*, σ_y^* effectively depend on the sum $E_+ + E_-$ due to the collider β -function chromaticity (the formula is valid to the first order of this effect and assumes the beam symmetry). According to (5), the mean collision energy $\langle W \rangle_L = \int wdL(E, w) \neq 2E$, which leads to the systematic error in the resonance mass.

The vertical dispersion $|\psi_y^*| \approx 800 \mu\text{m}$ with opposite signs for e^+ and e^- appears in VEPP-4M due to the beam separation in the additional interaction point. The residual orbit perturbations related to this separation result in the beam misalignment in the experimental I.P.

characterized by Δ_y . It leads simultaneously to the luminosity loss and the collision energy shift. To avoid that, the voltage on the experimental I.P. separator plates was tuned to have maximum luminosity in each run with the accuracy better than 3% so that $\Delta_y < 2.5 \mu\text{m}$ at the beam size $\sigma_y^* \simeq 7 \mu\text{m}$. Thus, the uncertainty of the collision energy W in the run is less than 10 keV for J/ψ and less than 18 keV for ψ' . In the resonance mass error, this uncertainty is suppressed $\propto 1/\sqrt{N}$, where $N > 100$ is the number of runs (see Sec. VIII).

The β -function chromaticity also leads to the shift of the mean value of the collision energy. For the given emittance ϵ_y , the vertical beam size $\sigma_y^* = \sqrt{\epsilon_y\beta_y^*}$. Using approximations $\beta_y(W/2) \approx \beta_y^*(1 + \partial \ln \beta_y^* / \partial E (W/2 - E))$ and

$$\frac{1}{\sqrt{1 + \partial \ln \beta_y^* / \partial E (W/2 - E)}} \approx \exp\left\{-\frac{1}{2}\partial \ln \beta_y^* / \partial E (W/2 - E)\right\} \quad (6)$$

in (5), one obtains $\delta \langle W \rangle = -1/4 \partial \ln \beta_y^* / \partial E \sigma_W^2$. The effect of the radial β -function chromaticity is suppressed by the factor of $(\sigma_{x,\beta}^* / \sigma_x^*)^2 \sim 0.1$ where $\sigma_{x,\beta}^*$ is the betatron radial size and σ_x^* is the total size including the dispersion. The $\beta^*(E)$ measurements at VEPP-4M gave the shifts of -4 ± 2 keV for J/ψ scans I–III, -1.5 ± 0.7 keV for J/ψ scan IV and $+5 \pm 2.5$ keV for ψ' (the chromaticity was partially compensated after the third scan of J/ψ).

At the 1 keV level of accuracy the potential energy of colliding particles inside the beams should be taken into account. The effective energy of the electron is $E_{kinetic} + U/2$, where the potential energy U is due to its Coulomb interaction with all other electrons of the beam. For the flat beam with the logarithmic accuracy

$$U = \frac{e^2 N}{\sqrt{\pi}\sigma_z} \ln \frac{D}{\sigma_x}, \quad (7)$$

where N is the bunch population, σ_z is the longitudinal bunch size and D is the beam pipe diameter (in the beam rest frame the interaction of particles at longer distances is screened out). The kinetic and potential energies in the I.P. differ from those in the ring because of the difference in the beam and beam pipe sizes, but the total energy conserves during the revolution, therefore

$$E_{kinetic, I.P.} + U_{I.P.}/2 = E_{kinetic, ring} + U_{ring}/2 \quad (8)$$

At the moment of the annihilation the total energy of the e^+e^- pair transforms to the product mass, thus

$$W = 2 \cdot (E_{kinetic, I.P.} + U_{I.P.}) = 2E_{kinetic, ring} + U_{ring} + U_{I.P.} \quad (9)$$

The resonant depolarization result is $\approx E_{kinetic, ring}$, therefore the collision energy shift $\delta W = U_{I.P.} + U_{ring}$. The energy losses ignored in this consideration does not change the final result.

For the the actual values of the beam currents and sizes it leads to a correction of (2 ± 1) keV for J/ψ and ψ' .

VI. EVENT SELECTION AND LUMINOSITY MEASUREMENTS

A. Detector and trigger

The KEDR detector [24] consists of the vertex detector, the drift chamber, the time-of-flight system of scintillation counters, the particle identification system based on the aerogel Cherenkov counters, the calorimeter (the liquid krypton in the barrel part and the CsI crystals in the end caps) and the muon tube system inside and outside of the magnet yoke. In this experiment the magnetic field was off and the liquid krypton calorimeter was out of operation.

To suppress the machine background to the acceptable level, the following trigger conditions were used by OR

1. signals from ≥ 2 barrel scintillation counters coinciding with the CsI calorimeter signal,
2. coinciding signals of two CsI end-caps,

with the CsI energy threshold of about 75 MeV. The Monte Carlo simulation employing the JETSET-7.4 code [25] yields the trigger efficiency of about 0.4 for J/ψ decays and about 0.43 for ψ' decays.

B. Multihadronic event selection

For the off-line event selection the following conditions were applied:

1. ≥ 3 charged tracks or 2 acolinear charged tracks ($\cos\theta < 0.95$) from the interaction region ($\rho < 5$ mm, $|z| < 120$ mm),
2. the CsI energy > 1.15 of the hardware threshold.

The second condition serves to exclude the hardware threshold instability. The detection efficiency, determined by the visible peak height and the table value of the leptonic width, is about 0.25 for J/ψ ($\sim 20 \cdot 10^3$ events) and about 0.28 for ψ' ($\sim 6 \cdot 10^3$ events).

The residual machine background (beam-gas and beam-wall) does not exceed 5 nb. The systematic error in the meson masses related to its variation is less

than 1 keV. To obtain this estimate, the background was increased by a few times by adding the appropriate fraction of unselected events to the selected ones at each experimental point (see Fig. 2). Further suppression of the background leads to the detection efficiency loss and does not improve the mass accuracy.

The meson mass value is rather sensitive to the detection efficiency variation during the energy scan, its reduction by 1% at one point causes the ψ' mass shift up to 5 keV. To ensure the detection efficiency stability, all electronic channels having problems at any moment of the experiment were *excluded from the off-line analysis*. Besides, the relative *hit efficiencies* of all detector subsystems were obtained for all experimental points using the cosmic ray runs, the multihadron event statistics and (when possible) background events. These efficiencies were applied to *the real multihadron events* to determine the relative point-specific correction factors. The variation of the drift chamber spatial resolution was handled similarly.

The correction procedure described above shifts the mass by $(+6.3 \pm 2.3)$ keV for J/ψ and $(+0.2 \pm 2.0)$ keV for ψ' . The errors include statistical errors of the hit efficiency determination and the uncertainties of the correction procedure employed. The shift of the J/ψ mass is mainly due to the false alarm of the safety system which stopped the gas flow in the drift chamber (one point of the second scan). The values of shifts are given just for information, only the errors are of importance.

C. Luminosity measurements

For the operative VEPP-4M luminosity measurements single bremsstrahlung monitors were installed in both e^+ - and e^- -directions. Their stability is not sufficient for the precision mass measurements, therefore Bhabha-scattering events detected by the end-cap CsI calorimeter were employed. The fiducial polar angle interval is $17.5^\circ < \theta < 35^\circ$. The resonance contribution is not negligible in this angular range, so that the $e^+e^- \rightarrow \psi \rightarrow e^+e^-$ and $e^+e^- \rightarrow e^+e^-$ interference should be taken into account. The correction to the number of e^+e^- -events has been included according to [26]. The values of the total and electronic widths were taken from [27] and the beam energy spreads were known from the experiment.

Unlike $e^+e^- \rightarrow \mu^+\mu^-$, the $e^+e^- \rightarrow e^+e^-$ interference dip is at the high-energy side of the resonance curve, so the mass shifts due to the correction are positive: (15 ± 1) keV (J/ψ) and (5 ± 0.5) keV (ψ').

To the errors quoted, 2 keV should be added for J/ψ and 3 keV for ψ' to cover the calorimeter instabilities.

VII. RESONANCE EXCITATION CURVE FITTING

A. Introduction

Taking into account the beam energy spread, the event production rate for the collider energy E can be written as

$$F(E) = \int \sigma(W) dL(E, W), \quad (10)$$

where W is the c.m. energy of the collision, $dL(E, W)$ is the differential luminosity and $\sigma(W)$ is the cross section.

In case of the narrow vector meson production in the reaction $e^+e^- \rightarrow V \rightarrow \text{hadrons}$

$$\sigma(W) = \frac{3\pi}{M^2} \int dx \times \frac{\Gamma_{ee}\Gamma_h}{(W(1-x) - M)^2 + \Gamma^2/4} \mathcal{F}(x, W), \quad (11)$$

where Γ , Γ_{ee} and Γ_h are total and partial widths of the meson, M is its mass and $\mathcal{F}(x, W)$ is the probability to lose the fraction of energy x because of the initial state radiation [28] (we substituted the Breit-Wigner cross section with the physical value of Γ_{ee} including the vacuum polarization effects and used W instead of $s = W^2$).

After the corrections introduced in Sec. V to exclude the asymmetry causing the resonance mass shift, the symmetric expression for the differential luminosity can be used:

$$\frac{dL(E, W)}{dW} \approx \frac{L}{\sqrt{2\pi}\sigma_W(I, \mathcal{J})} \times \exp\left\{-\frac{(W-2E)^2}{2\sigma_W^2(I, \mathcal{J})}\right\}, \quad (12)$$

where the (free) small parameter k is introduced to cover non-gaussian effects due to the β -function chromaticity and other possible reasons. The collision energy spread σ_W can depend on the beam current I because of the microwave instability reviewed in [29] and/or on the current density \mathcal{J} due to the multiple intra-beam scattering ([30] and references therein). The latter depends not only on the beam current, but also on the beam sizes modifying substantially by the collision effects, thus it must be considered as an independent parameter.

Formula (11) ignores the interference between the resonant and nonresonant hadron production. With the sufficient accuracy [26]:

$$\sigma(W) = \frac{12\pi}{M^2} \left\{ \left(1 + \frac{3}{4}\beta\right) \frac{\Gamma_{ee}\Gamma_h}{\Gamma M} \cdot \text{Im}f - \left(1 + \frac{11}{12}\beta\right) \frac{2\alpha\sqrt{R}\Gamma_{ee}\Gamma_h}{3M} \lambda \cdot \text{Re}f \right\}. \quad (13)$$

Here α is the fine structure constant, $R = \sigma^{(h)}/\sigma^{(\mu\mu)}$,

λ denotes the fraction of events interfering with the non-resonant hadronic cross section and

$$\beta = \frac{4\alpha}{\pi} \left(\ln \frac{W}{m_e} - \frac{1}{2} \right), \quad f = \left(\frac{M/2}{-W + M - i\Gamma/2} \right)^{1-\beta}.$$

In the limit of zero resonance width $\Gamma \rightarrow 0$, assuming the Gaussian energy spread and ignoring the interference, it is possible to express (10) in terms of known functions:

$$F(E) = \frac{6\pi^2}{M^2} \frac{\Gamma_{ee}\Gamma_h}{\Gamma} \left(\frac{2\sigma_W}{M} \right)^\beta \times \frac{\Gamma(1+\beta)}{\sqrt{2\pi}\sigma_W} \exp\left\{-\frac{(W-2E)^2}{4\sigma_W^2}\right\} \times D_{-\beta}\left(-\frac{W-2E}{\sigma_W}\right) (1+\delta) L, \quad (14)$$

where Γ is the gamma-function, $D_{-\beta}$ is the Weber parabolic cylinder function and

$$\delta = \frac{\alpha}{\pi} \left(\frac{\pi^2}{3} - \frac{1}{2} \right) + \frac{3}{4}\beta.$$

B. Interference effect treatment

In principle, the interference magnitude can be left free in the fit and extracted from the data together with the resonance mass and the machine energy spread σ_W . Unfortunately, this affects too much the statistical accuracy of the mass measurements, so one has to fix it. The zero magnitude is usually assumed.

In this analysis we fix the interference parameter λ , employing the parton model of the onium decays. It assumes that J/ψ decays to the light $q\bar{q}$ -pairs with the probability of $RB_{\mu\mu}$ and to the gluon triplet ggg or the $gg\gamma$ mixture with the probability of $1 - (R+2)B_{\mu\mu}$, where $B_{\mu\mu}$ is the muon branching ratio. The events $J/\psi \rightarrow q\bar{q}$ are identical to those in the non-resonant continuum, and there is the 100% interference in this case. For the hypothetical heavy onium decays, ggg - $q\bar{q}$ interference is negligible due to the difference in the angular distributions (three jets vs two jets). For the real J/ψ , the angular distributions do not differ much but the interference phases are individual for all exclusive final states, therefore the net interference effect should be small just because of the large number of decay modes.

So, the fraction of multihadron J/ψ decay events interfering with the continuum $\lambda \approx RB_{\mu\mu}/(1-2B_{\mu\mu}) \approx 0.17$. The uncertainty of λ related to the final number of the decay modes was estimated by the multiple assignment of the arbitrary interference phases to all J/ψ and ψ' decay modes implemented in the JETSET-7.4 Monte Carlo code [25]. The following values have been obtained: $\lambda_{J/\psi} = 0.17 \pm 0.03$ and $\lambda_{\psi'} = 0.023 \pm 0.009$. The corresponding mass shifts are $(+7.0 \pm 1.3)$ keV and $(+2.0 \pm 0.8)$ keV, respectively. The accuracy of the parton model predictions used gives a small addition to the

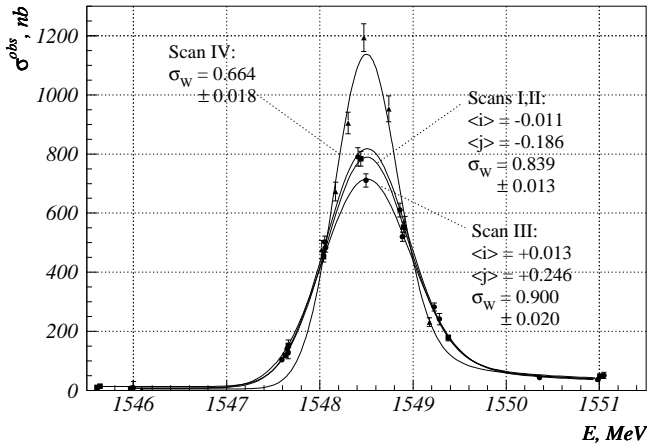


FIG. 7: The results of four J/ψ scans (the energy spread values σ_W and the mean i, j values for the first two and the third scans are presented).

errors quoted. The fitting procedure automatically shifts the mass value so only the errors of the quoted values are of importance.

C. On collision energy spread variations

The single beam measurements of the longitudinal and radial bunch sizes indicate that the energy spread in VEPP-4M depends on the bunch current. In the J/ψ region the dimensionless slope $(d\sigma_E/\sigma_E)/(dI/\langle I \rangle) \simeq 0.07$. As the current decreases during the run, it leads to the symmetric distortion of the collision energy distribution and contributes to the k parameter of (12). If the mean value of the energy spread is not the same at all energy points where data were collected, the fake mass shift can appear.

To take into account the energy spread variations in the resonance curve fit, we assumed that it linearly depends on the beam current and the current density in the vicinity of their mean values

$$\begin{aligned} \sigma_E &\approx \langle \sigma_E \rangle (1 + \alpha_i \cdot i + \alpha_j \cdot j), \\ i &= \frac{I}{\langle I \rangle} - 1, \quad j = \frac{\mathcal{J}}{\langle \mathcal{J} \rangle} - 1. \end{aligned} \quad (15)$$

The product $I \cdot \ell^n$ with the specific luminosity $\ell = L/I_+I_- \propto 1/\sigma_x^*\sigma_y^*$ were chosen as a measure of the current density effect as the beam sizes in the ring were not permanently monitored. The α_i and α_j were considered as free parameters, the values $n = 2$ and $n = 1$ were tried. If the synchrotron contribution in the radial size dominates, and the vertical beam size is due to the coupling ($\sigma_y^* \propto \sigma_{x\beta}^*$), one has $n = 2$ for the multiple intra-beam scattering. With $n = 1$ the j parameter just characterizes the strength of the collision effects ($I\ell \propto \xi_y$ for the flat beams).

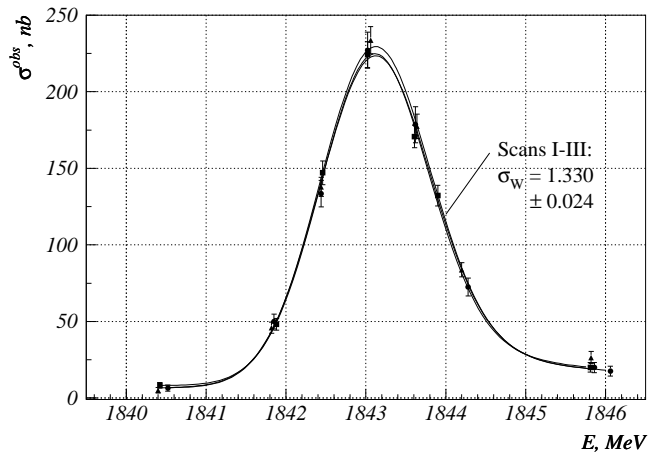


FIG. 8: The results of three ψ' scans (the mean energy spread value σ_W is presented).

D. Fitting procedure

Each data acquisition run was subdivided into subruns with a minor variation of the beam currents. For each subrun the beam energy E was assigned and the parameters i_{\pm} and j_{\pm} were calculated for the e^+ - and e^- -beams.

The observed number of the multihadron events N has been fitted as the function of E , i and/or j using the log-likelihood method. The calculations of the expected number of the resonance events were performed by the numerical convolution of (13) and (12) with $\sigma_W = \sqrt{\sigma_{E+}^2 + \sigma_{E-}^2}$ depending on i_{\pm} and/or j_{\pm} according to (15). The free parameters were: the constant *continuum cross section* σ_c , the event *detection efficiency* ϵ for the given value of the leptonic width Γ_{ee} , the *resonance mass* M and the *energy spread parameters* $\langle \sigma_W \rangle$, α_i and/or α_j . The PDG table values [27] were used for the resonance widths Γ and Γ_{ee} . The λ parameter in (13) was fixed as described above.

For the fitting procedure verification and the systematic error checks, $N(E)$ fits were performed using (14) with the results presented in Fig. 7 and Fig. 8.

The peak height for the third J/ψ scan differs from those for the first and the second ones due to the σ_W dependence on the parameter j . The energy spread in the fourth scan was decreased intentionally (see Sec. III).

In the ψ' case, the energy spread variations are not seen due to higher energy and narrower i, j -ranges.

The chi-squared values of the fits are satisfactory ($P(\chi^2) > 0.1$) for all J/ψ and ψ' scans even if the dependence of the energy spread on the beam current within a scan is ignored.

The detection efficiencies obtained by the fit assuming the world average values of the leptonic widths $\Gamma_{ee, J/\psi} = 5.26 \pm 0.37$ keV, $\Gamma_{ee, \psi'} = 2.19 \pm 0.15$ keV [27] agree with those obtained by Monte Carlo simulation within their errors. The systematic error of the Monte

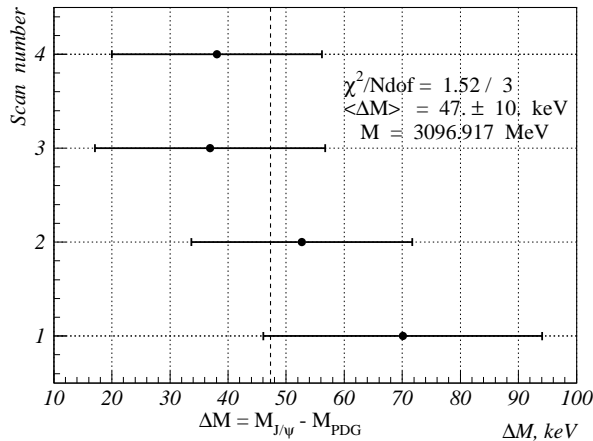


FIG. 9: J/ψ mass values for each scan relative to the world average value [27], the resulting average values are shown by the dashed lines (statistical errors only).

Carlo calculations and the error of the absolute luminosity calibrations in this experiment are large (about 12% in total), so we do not present our leptonic width values. For the mass measurements these errors are not important.

VIII. MEASURED MASS VALUES AND ERROR DISCUSSION

The mass values obtained in each scan *assuming the constant value of σ_W during a scan* and the resulting average mass values for J/ψ and ψ' as well as their statistical errors are presented in Figs. 9,10.

To obtain the resulting averaged mass values, the scans were considered as independent experiments. The individual mass values of the scans were weighted using their statistical errors and ignoring the systematic ones. Correspondingly the systematic errors of the individual scans were weighted. Such procedure overestimates the total error, but allows one to separate the statistical and systematic errors of the resulting value.

The mass values for all scans are in good agreement even when the difference in systematic errors is ignored (the χ^2 is given in Figs. 9,10). The resulting statistical accuracy is 10 keV for J/ψ and 25 keV for ψ' .

The fit of J/ψ scans I÷III does not show the statistically significant direct dependence on I ($\alpha_i = 0.037 \pm 0.055$) and gives the dimensionless slope $\alpha_j = 0.059 \pm 0.018$ similar to that of the single-beam measurements. The mass deviation from the value for $\alpha_i, \alpha_j = 0$ does not exceed 1.5 keV. The correction is rather small, so the mass values for $\alpha_i, \alpha_j = 0$ have been assigned to the scans I-III of J/ψ with the systematic error of 1.5 keV related to the energy spread variations.

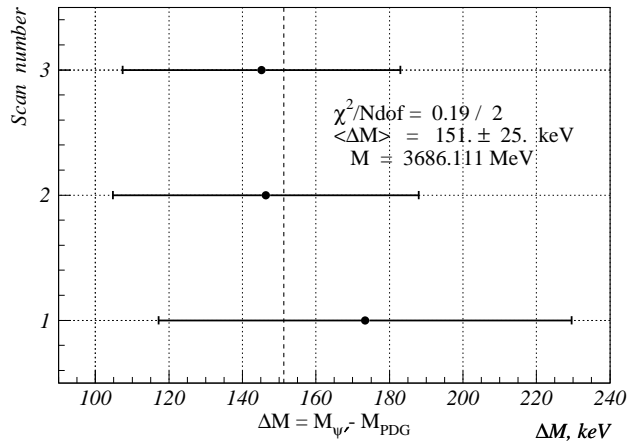


FIG. 10: ψ' mass values for each scan relative to the world average value [27], the resulting average values are shown by the dashed lines (statistical errors only).

For the J/ψ scan IV with the damping decrements rearranged, one has $\alpha_j = 0.45 \pm 0.15$ for α_i fixed at zero and $\alpha_i = -0.13 \pm 0.16$ for α_j fixed at zero with the mass variations of +10 keV and -8 keV, respectively. The mass value for $\alpha_i, \alpha_j = 0$ has been assigned to the scan IV of J/ψ with the systematic error of 10 keV related to the energy spread variations. The mass value obtained assuming the dependence on $J \propto I \cdot \ell^1$ does not contradict to this error estimate. The difference of the J/ψ mass values obtained in the scan IV and in the scans I÷III is $(-11 \pm 22 \pm 12)$ keV.

The systematic uncertainties are listed in Table III. The sources of uncertainties not exceeding 0.3 keV (the uncertainties of the world average values of particle properties used, the resonance mass uncertainty related to (4), the radiative corrections uncertainties etc.) are omitted.

The weighted contribution of the energy spread variation to the systematic error of the resulting J/ψ mass value is about 3 keV. During the ψ' scans, the statistically significant variations of the energy spread have not been observed, a relatively big systematic error of 2 keV is due to the bigger value of σ_W .

The uncertainty of the energy assignment includes the statistical component which was estimated using the multiple data fits with a randomly generated energy deviation. The systematic contribution consists of two parts. The first one is related to the energy prediction function (p.f.) choice and the energy assignment policy. Three values of energy were tried for each run: the unbiased p.f. value and two values of the shifted p.f. which exactly reproduce the preceding and following calibration results. Besides, the best p.f. parameter variation within their errors were allowed and a few different functions were tried. The second part is due to the difference between the data acquisition runs and the energy calibration runs

TABLE III: The systematic uncertainties in J/ψ and ψ' masses (keV)

<i>Source</i>	J/ψ	ψ'
Energy spread variation (Sec. VIII, VII C)	3.0	2.0
Energy assignment: statistical uncertainty (Sec. VIII, IV B)	2.5	3.5
Energy assignment: prediction function choice (Sec. VIII, IV B)	2.7	1.7
Energy assignment: radial betatron oscillations (Sec. IV B)	< 1.5	< 1.8
Energy assignment: beam separation in the additional I.P. (Sec. IV B)	0.4*	0.4*
Beam misalignment in the interaction point (Sec. V)	1.8	5.1
e^+ -, e^- -energy difference (Sec. VIII)	< 2.0	< 2.0
Non-gaussian collision energy distribution (Sec. VIII, VII A)	< 1.5	< 2.0
β -function chromaticity (Sec. V)	2.0*	2.5*
Beam potential (Sec. V)	1.0*	1.0*
Single energy calibration (Sec. II C)	0.6	0.8
Detection efficiency instability (Sec. VI B)	2.3	2.0
Luminosity measurements (Sec. VI C)	2.2	3.0
Interference in the hadronic channel (Sec. VII B)	1.3	0.8
Residual machine background (Sec. VI B)	< 1.0	< 1.0
<i>Sum in quadrature</i>	≈ 7.3	≈ 8.9

* — correction uncertainty

TABLE IV: The corrections applied to the J/ψ and ψ' mass values (keV).

<i>Correction for</i>	J/ψ (I÷III)	J/ψ (IV)	ψ'
Vertical orbit disturbances (Sec. II C)	-0.8 ± 0.6	-0.8 ± 0.6	-0.6 ± 0.4
Separation in the additional I.P. (Sec. IV B)	-3.4 ± 0.4	-3.4 ± 0.4	-4.0 ± 0.4
β -function chromaticity (Sec. V)	-4.0 ± 2.0	-1.5 ± 0.7	5.0 ± 2.5
Beam potential (Sec. V)	1.9 ± 1.0	2.1 ± 1.0	2.0 ± 1.0
<i>Total</i>	-6.3 ± 2.4	-3.6 ± 1.7	1.4 ± 2.8

(the radial betatron oscillations and the separation in the additional I.P., Sec. IV B).

The mass uncertainty caused by the beam misalignment in the experimental I.P. and the electrostatic dispersion was evaluated similarly to that of the statistical error of the energy assignment.

Estimates show that the difference of the energies of e^+ - and e^- -beams is small. The value shown in Table III has been obtained using a few energy calibrations with the e^+ -beam performed during the stability runs (Sec. IV A).

The symmetric distortion of the distribution in the collision energy W can shift the mass due to the asymmetry of radiative corrections. The corresponding uncertainty has been estimated by leaving the k parameter of (12) free (the values shown in Fig. 9,10 are for $k = 0$).

All other sources of the systematic error were discussed above. The resulting systematic error in the mass is about 7 keV for J/ψ and about 9 keV for ψ' . The corrections applied to the fit results are presented in Table IV.

The results obtained can be presented in the form

$$\begin{aligned}
 M_{J/\psi} - M_{J/\psi}^{PDG} &= 47 \pm 10 \pm 7 (\pm 40 [27]) \text{ keV}, \\
 M_{\psi'} - M_{\psi'}^{PDG} &= 151 \pm 25 \pm 9 (\pm 90 [27]) \text{ keV},
 \end{aligned}$$

demonstrating the agreement with the world average values.

IX. CONCLUSION

The new high precision measurement of the J/ψ - and ψ' -meson masses has been performed at the collider VEPP-4M using the KEDR detector. The following mass values have been obtained:

$$\begin{aligned}
 M_{J/\psi} &= 3096.917 \pm 0.010 \pm 0.007 \text{ MeV} \\
 M_{\psi'} &= 3686.111 \pm 0.025 \pm 0.009 \text{ MeV}
 \end{aligned}$$

The relative measurement accuracy reached $4 \cdot 10^{-6}$ for J/ψ , $7 \cdot 10^{-6}$ for ψ' and is approximately 3 times better than that of the previous precise experiments.

For the mass difference our result is

$$M_{\psi'} - M_{J/\psi} = 589.194 \pm 0.027 \pm 0.011 \text{ MeV}.$$

Acknowledgments

We greatly appreciate the efforts of the staff of VEPP-4M to provide good operation of the complex and the staff of experimental laboratories for permanent support during preparation and performing this experiment. The authors express their special gratitude to V.S. Fadin and A.I. Milstein for the theoretical support and Yu.M. Shatunov for stimulating discussions.

-
- [1] A. A. Zholents et al. (OLYA Collaboration), Phys. Lett. **B96**, 214 (1990).
- [2] A. S. Artamonov et al. (MD-1 Collaboration), Phys. Lett. **B118**, 225 (1982).
- [3] A. S. Artamonov et al. (MD-1 Collaboration), Phys. Lett. **B173**, 272 (1984).
- [4] S. E. Baru et al. (MD-1 Collaboration), Z. Phys. **C56**, 547 (1992).
- [5] S. E. Baru et al. (MD-1 Collaboration), Phys. Rep. **267**, 71 (1996).
- [6] S. E. Baru et al. (Symposium on Twenty Beautiful Years Of Bottom Physics, Chicago, 1997), p. 97.
- [7] A. S. Artamonov et al. (OLYA and MD-1 Collaboration), Phys. Lett. **B474**, 427 (2000).
- [8] E. R. Cohen and B. N. Taylor, J. Phys. Chem. Reference Data **2**, 663 (1973).
- [9] E. R. Cohen and B. Taylor, Rev. Mod. Phys. **59**, 1121 (1987).
- [10] A. D. Bukin et al. (Vth intern. Symp. on High energy physics and elementary particle physics, Warsaw, 1975), p. 138.
- [11] Y. S. Derbenev et al., Particle Accelerators **10**, 177 (1980).
- [12] W. W. MacKay et al. (CUSB collaboration), Phys. Rev. **D29**, 2483 (1984).
- [13] D. P. Barber et al. (ARGUS collaboration), Phys. Lett. **B135**, 498 (1984).
- [14] T. A. Armstrong et al. (E760 Collaboration), Phys. Rev. **D47**, 772 (1993).
- [15] J. Bai et al. (BES Collaboration), Phys. Rev. Lett. **69**, 3021 (1992).
- [16] A. A. Sokolov and I. M. Ternov, Sov. Phys. Dokl. **18**, 1203 (1964).
- [17] A. P. Lysenko, A. A. Polunin, and Y. M. Shatunov, Part. Accel. **18**, 215 (1986).
- [18] A. N. Skrinsky and Y. M. Shatunov, Sov. Phys. Usp. **32**, 548 (1989).
- [19] C. Bernardini et al., Phys. Rev. Lett. **10**, 407 (1963).
- [20] V. E. Blinov et al. (European Particle Acceleration Conference, Paris, 2002), p. 1954.
- [21] V. E. Blinov et al. (Particle Acceleration Conference, Chicago, 2001), p. 3317.
- [22] V. E. Blinov et al., Nucl. Inst. & Meth. **A494**, 68 (2002).
- [23] A. V. Bogomyagkov et al. (European Particle Acceleration Conference, Paris, 2002), p. 396.
- [24] V. V. Anashin et al., Nucl. Inst. & Meth. **A478**, 420 (2002).
- [25] T. Sjostrand and M. Bengtsson, Comp. Phys. Comm. **43**, 367 (1987), CERN-TH.7112/93.
- [26] Y. I. Asimov et al., Pisma Zh. Eksp. Teor. Fiz. **21**, 378 (1975), [Ya. I. Asimov et al., JETP Lett. **21**, 172 (1975)].
- [27] K. Hagiwara et al. (Particle Data Group), Phys. Rev. **D66**, 010001 (2002).
- [28] E. A. Kuraev and V. S. Fadin, Sov. J. Nucl. Phys. **41**, 466 (1985), [E. A. Kuraev and V. S. Fadin, Yad. Fiz. **41**, 733 (1985)].
- [29] E. Shaposhnikova, CERN-SL-99-8-HRF (1999), prepared for Joint US-CERN-Japan-Russia School on Particle Accelerators: Beam Measurement, Montreux, Switzerland, 11- 20 May 1998.
- [30] K. L. F. Bane et al., Phys. Rev. ST Accel. Beams **5**, 084403 (2002), physics/0206003.